INTERNATIONAL ATOMIC ENERGY AGENCY
UNITED NATIONS EDUCATIONAL, SCIENTIFIC AND CULTURAL ORGANIZATION

INTERNATIONAL CENTRE FOR THEORETICAL PHYSICS
34100 TRIESTE (ITALY) - P.O.B. 586 - MIRAMARE - STRADA COSTIERA 11 - TELEPHONE: 2240-1
CABLE: CENTRATOM - TELEX 460392 - I

SMR/208 - 40

SPRING COLLEGE IN MATERIALS SCIENCE

ON

"METALLIC MATERIALS"

(11 May - 19 June 1987)

SURFACE TREATMENT AND COATINGS OF MATERIALS
(Part IV)

R. BULLOUGH
Materials Development Division
B552 Harwell Laboratory
Oxfordshire OX11 ORA
U.K.

These are preliminary lecture notes, intended only for distribution to participants.

LECTURE 4

INTERFACES AND STRESSES

Abstract

The nature of the interface between a coating and its parent substrate and the presence of residual stress in a coating can critically affect the performance of the coating in service. For example, if significant interdiffusion occurs between the overlayer and the substrate, then long-term life can be affected. Additionally, if a hard coating is deposited onto a soft substrate, then the perceived advantage of having such a hard coating may well be held in question if the overlayer is too thin. In addition, if the residual stress in a ceramic coating is highly tensile, then failure in service is highly likely. These synergistic aspects will be discussed in this lecture.

Slide 1 — TITLE SLIDE : Interfaces and Stresses

Slide 2 — HR16814

Slide 3 — Plasma sprayed coatings.

Slide 4 — As sprayed, ceramic artefacts may fail unexpectedly without the application of any external stress as a result of the stresses built in during processing. Such stresses can lead to the complete failure of the component as shown in this slide.

Slide 5 — In advanced gas turbine engines, the use of ceramic coatings on turbine blades is a route to increasing the operating temperature of the engine and, therefore, the thermodynamic efficiency. This slide shows representative examples of zirconia coated turbine blades immediately after coating.

Slide 6 — Clearly, the performance of the coating and turbine blade has to be established under typical operating conditions. This slide shows coated turbine blades after exposure to 1100°C for extended periods of time. It is important to note that the coating has begun to fail at the interface with the metal substrate and that the metal substrate has oxidised badly.

Slide 7 — Closer examination of a typical ceramic microstructure reveals the presence of microcracks prior to failure. These microcracks are the precursor to catastrophic failure and arise from the combination of deposition and environmental stresses.

Slide 8 — In order to establish the likely magnitudes and sensitivities of the residual stress in the coating, it is important to model the deposition process. Essentially, a major part of the problem reduces to building a heat transfer model of the heat input to the substrate and coating during the growth of the coating by the addition of molten ceramic particles. A range of process parameters can then be explored to determine which will critically affect the stress in the coating.

Slide 9 — A parameter which is influential is the initial substrate temperature. This affects the coating stress through the expansion mismatch between the substrate and the coating. It is clear that even modest increases in substrate temperature can induce a factor of 3 increase in the residual stress in the coating.

Slide 10 — The thermal conductivity of the coating is also a critical parameter as shown in this slide where a change of only 25% in the thermal conductivity can completely reverse the sign of the stress in the coating.

Slide 11 — The rate at which the coating is deposited is another influential parameter and may again lead to the stress changing from being compressive to tensile. For a brittle material such as a ceramic, tensile stresses are to be avoided since they lead to crack growth and rapid failure.

Slide 12 — The coating thickness can also have a dramatic effect on the stress distribution across a zirconia coating deposited by plasma spraying. This theoretical prediction correlates well with experimental experience where it is known that to deposit zirconia by this technique at a thickness of approximately 2.5mm can lead to the onset of rapid and unexpected failure of the coating after deposition.

Slide 13

Similarly, it is important to recognise that the simple act of producing a thick coating does not necessarily lead to a linear increase in fracture stress as this slide demonstrates. It is also important to note that because the coating contains defects (such as porosity and cracks), these will act as stress concentrators and may lead to a lowering of the fracture stress of the ceramic coating compared to a bulk material of the same composition.

Slide 14

As well as optimising process variables in order to minimise residual stresses in coatings, it is possible to change the chemistry of the material which affects the interatomic binding forces through the fracture stress. In this example, it can be seen that the concentration of yttria in yttria stabilised zirconia (YSZ) can change the fracture stress by approximately 50%. Equally, it is important to deposit the coating in a continuous fashion rather than trying to build up successive layers since the latter approach introduces additional planar interfaces which act as weak boundaries when a stress is applied.

Slide 15

LINK SLIDE : "Physical Vapour Deposition : Stresses and Interfaces"

Slide 16

Normally, physical vapour deposition (PVD) is used to deposit thin films (less than 60μm thick) as shown in this typical example of titanium nitride coatings about 2μm on cutting tools. Stresses can also be built up in these thin layers and, given the harsh working environment, a knowledge of the residual stresses is important in determining the quality of the composite material.

Slide 17

Classically, residual stresses in these thin film media can be measured by X-ray techniques as shown schematically in this slide. An X-ray beam is diffracted from a set of crystallographic planes and the change in interplanar spacing is measured as a function of the angle of tilt of the film to the X-ray beam.

Slide 18

The results can be conveniently plotted as the dimensionless parameter strain v. the square of the sign of the tilt angle. Typical results are shown in this slide where it is clear that the substrate can critically affect the stress which is measured in the titanium nitride coating.

Slide 19

It is also possible to separate the expansion mismatch stress from the deposition stress as shown in this example. It is clear that the thermal contribution to the internal stress can be significant.

Slide 20

The effect that residual stress can have on the microstructure of a coating is also evident from this slide. Photograph A shows that at the interface with the substrate, the microstructure consists of small densely packed grains, whilst at the outer surface as shown in photograph B, the grains are larger and more separated.

Slide 21

As a result, it is possible to predict that the yield stress of the material will vary as a function of position within the coating as shown by this schematic slide.

Slides 22/23

The importance of thermal stresses to the densification of PVD coatings is illustrated in these next two slides. For a Molybdenum coating deposited onto Molybdenum, then there is obviously no thermal stress and the right-hand micrograph shows quite open boundaries between the grain crystallites. However, for a similar coating deposited onto stainless steel, a large thermal stress component is generated and the high magnification scanning electron micrograph on the right shows a very dense microstructure has developed as a result.

Slide 24

The importance of internal stress in the densification of PVD coatings cannot be over-emphasised and for ceramic coatings this effect is also particularly important. On the left is a carbide coating which shows a very dense microstructure; by removal of the substrate constraint on the right, the open boundaries typical of the structured diagrams illustrated in a previous talk can be seen.

Slide 25

Due to the large compressive stress in the plane of the foil of titanium nitride coatings, a Poisson's ratio expansion of lattice planes parallel to the coating substrate interface is obtained. Therefore, the increase in unit cell dimension for titanium nitride coatings correlates well with this large internal stress.

Slide 26

Again, removal of the substrate constraint causes complete relaxation of internal stress and the lattice parameter of the titanium nitride coatings, irrespective of substrate, fall to their unstressed values.

Slide 27

LINK SLIDE : "Interface Phenomena"

Slide 28

We have already seen in the lecture on "Thin Film Properties" that the adhesion of a thin film can be measured in comparative terms using a scratch tester. As has also been pointed out in the presentation on "Microstructures", the initial interface which is presented for coating should be clean and free from second-phase species. In PVD processing, it is possible to clean this interface by ion bombardment and, as the results show, the adhesive force between the coating and the substrate is strongly dependent on the ion cleaning step.

Slide 29

These photographs show that ion cleaning a substrate and then depositing a coating (photograph B) produces a uniform fracture, whereas (photograph A) a non-cleaned surface fractures in a discontinuous manner as a result of stress concentration effects at the interface with the substrate.

Slide 30

In certain cases it is possible to introduce an additional coating between the titanium nitride and the substrate to increase the adhesive force. In this particular case, titanium shows a beneficial effect when deposited underneath titanium nitride onto an M2 tool steel. Again, however, the thickness of the layer is important as this can affect the stress in the layer.

Slide 31

Thin film coatings can also be used in advanced heat engines. For example, this slide of a diesel engine exhaust valve shows the beneficial effect of adding a coating to the head to reduce oxidation of the valve steel.

Slide 32

Detailed examination of the coated steel after thermal exposure shows that the elements of the coating (in this case, iron, chromium, aluminium and yttrium) can redistribute into the substrate and up to the free surface as noted previously in the lecture on "Microstructures".

Slide 33

Detailed microanalysis reveals the extent to which this distribution can take place.

Slide 34

Further interfacial studies reveal that the interdiffusion region can change crystal structure as a result of the ingress of elements which, for example, stabilise a face-centred cubic as against a body-centred cubic crystal structure.

Slide 35

The extent of diffusion into the substrate can be limited by the use of diffusion barriers. For example, the titanium nitride interlayer in this case has reduced the diffusion of the coating into the substrate. Additionally, however, porosity has developed as elements from the substrate can still diffuse into the coating leaving behind vacancies which then form voids.

Slide 36

The retardation of interdiffusion effects by titanium nitride interlayers is clearly shown in this slide. The open square shows the reduced interdiffusion of aluminium into a stainless steel substrate, whilst the full squares show the extent of interdiffusion in the absence of a diffusion barrier.

Slide 37

This work is of great importance to the gas turbine industry as failure at interfaces can mean the loss of performance in, for example, a Harrier vertical take-off and landing engine. The turbine blades in the centre of this slide are intended for such an engine.

Slide 38

On exposure to high temperatures, a number of changes occur within the coating and the substrate and these are illustrated in this slide. For example, reactive elements such as aluminium and chromium migrate to the free surface to form protective oxidation resistant oxide scales. Similarly, some elements will migrate to the substrate to form intermetallic precipitates and phase changes.

Slides 39/40

All these processes are diffusion rate limited and at high temperatures these effects can be quite significant as shown by these two slides. At lower temperatures, these effects become less of a problem to engine designers as the thermodynamic driving force is reduced.

Slide 41

The square of the interdiffusion distance when plotted against time is a linear diffusion confirming that the processes are indeed diffusion rate limited.

Slide 42

During the deposition of these oxidation corrosion resistant coatings, surface topography plays an important role in the nucleation and growth phase of the deposit. Surface irregularities can lead to the formation of so-called leader defects which must be eliminated from the microstructure to guarantee performance.

Slide 43

This slide illustrates a leader defect in an advanced alloy coating. The interfaces in the coating which can give rise to problems can also be between the columnar grains as shown in this slide where, during high temperature oxidation, a defect between the columnar grains has led to the preferential ingress of oxygen, and therefore oxidation of the coating deep inside the microstructure.

Slide 44

It is important to further process these oxidation resistant coatings and this is carried out in two ways. This slide shows if the microstructure is heat-treated and then glass bead peened to close off defects, then thermal cracking is initiated after 300 cycles.

Slide 45

Optical metallography shows these thermal cracks extend deep into the coating.

Slide 46

However, if the microstructure is peened and then heat-treated, no cracking occurs after 500 cycles.

Slide 47

It is only after 1,200 cycles that evidence of thermal fatigue cracks is seen.

Slide 48

Optical metallography shows these thermal fatigue cracks extend deep into the microstructure of the coating and penetrate into the substrate. The improvement in performance by peening and then heat-treating is that good metallurgical bonds are formed between the interfaces of the columnar grains, thereby eliminating leader defects.

Slide 49

SUMMARY SLIDE

The main points arising out of this lecture are that the stress induced in a coating as a result of deposition can be significant and can lead to failure of the coating. Advanced techniques are required to assess the quality of these coatings. The interfaces between the coating and the operating environment and the coating and the substrate are critical. Growth defects are also very important and may lead to premature failure along interfacial boundaries.

INTERFACES AND STRESSES

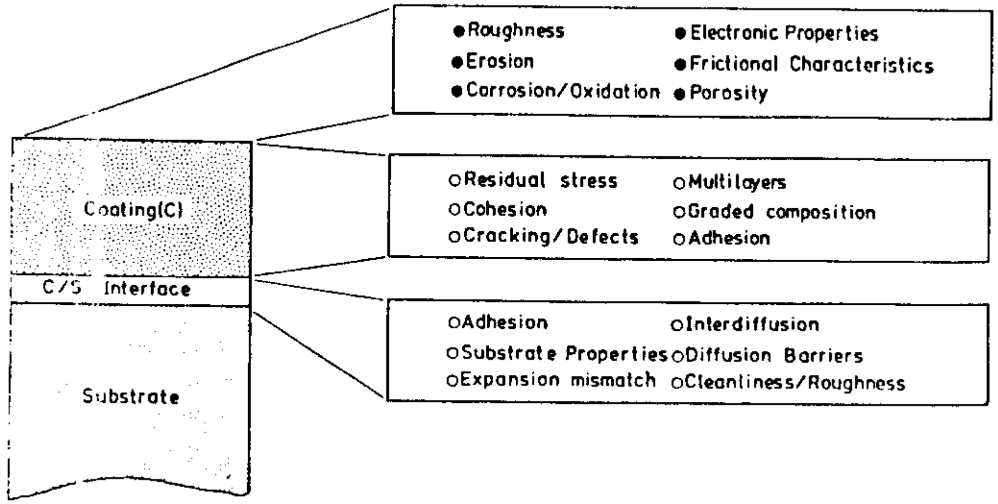

1. Interfaces and Stresses

PLASMA SPRAYED COATINGS

Ceramic artefact – failed due to built in stress during forming. No external stress.

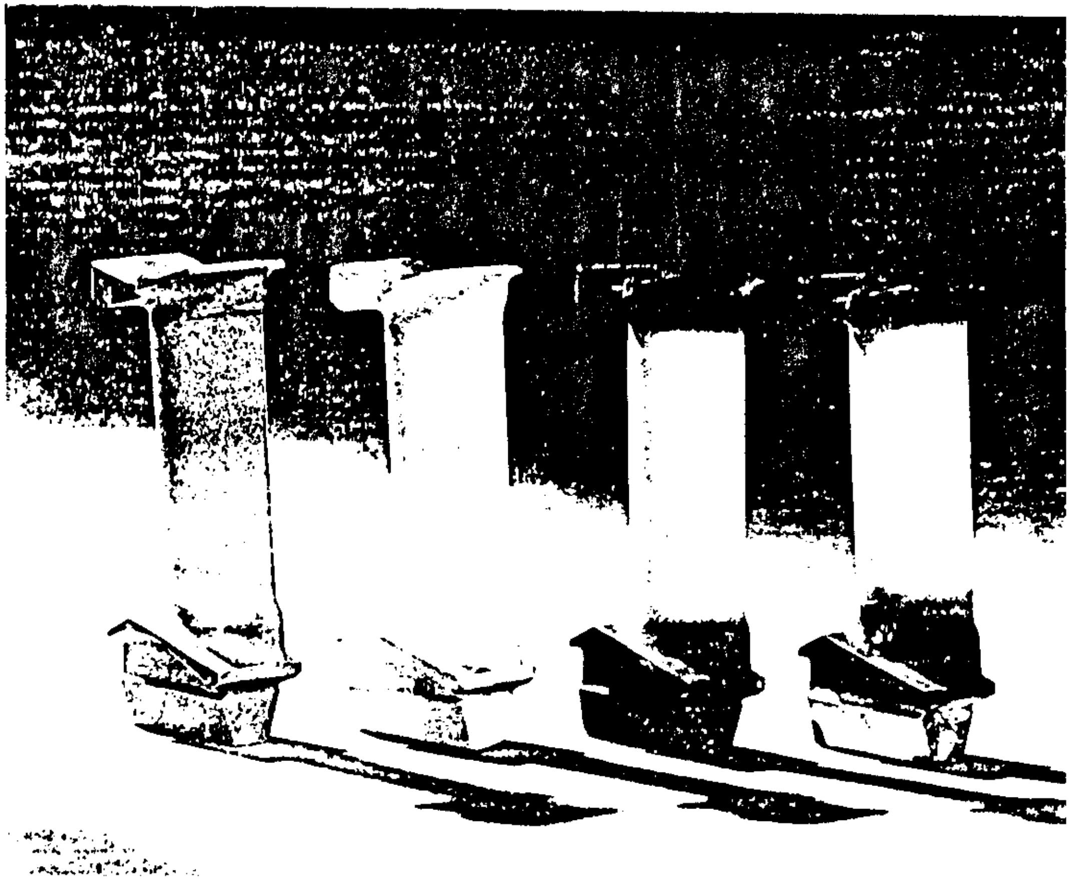

Representative ZrO_2 coated turbine blade immediately after coating – increases operating T of engine – leading to greater efficiency (thermodynamic)

LECTURE 4 : SLIDE 6

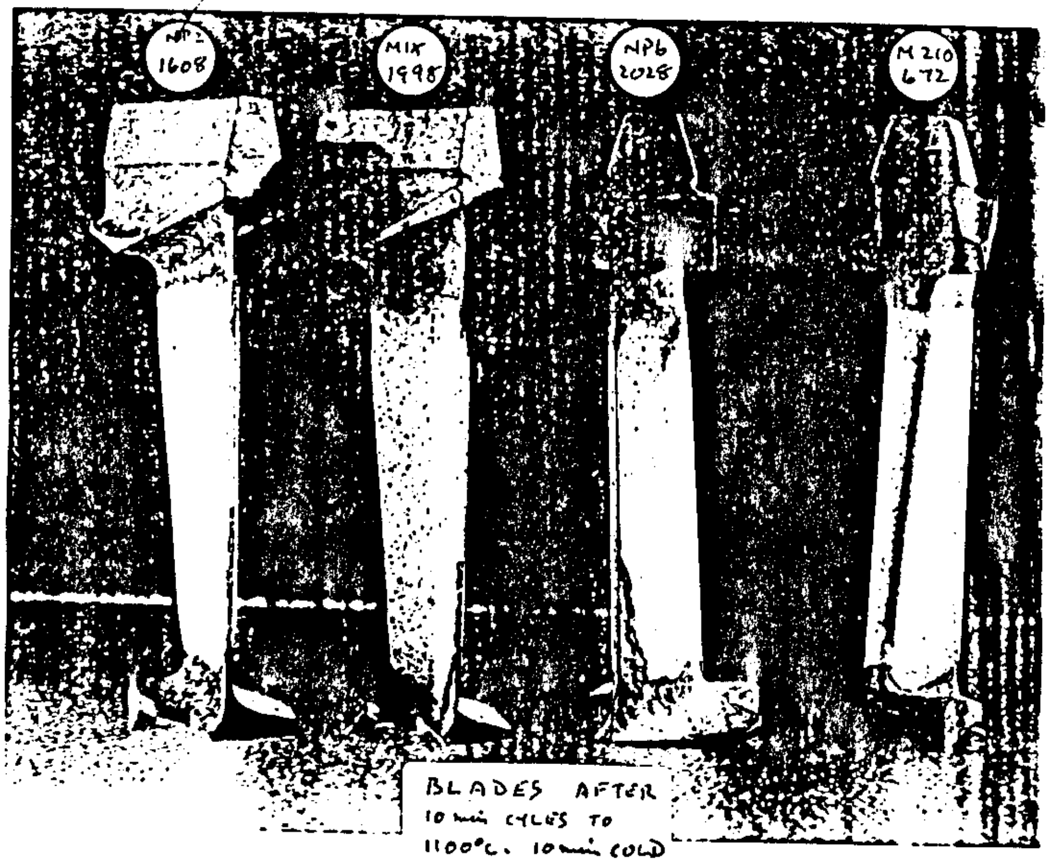

ZrO₂

Coating failing after cyclic heating.

Note failure is at the interface

LECTURE 4 : SLIDE 7

Precursor micro cracks in the coating

LECTURE 4 : SLIDE 8

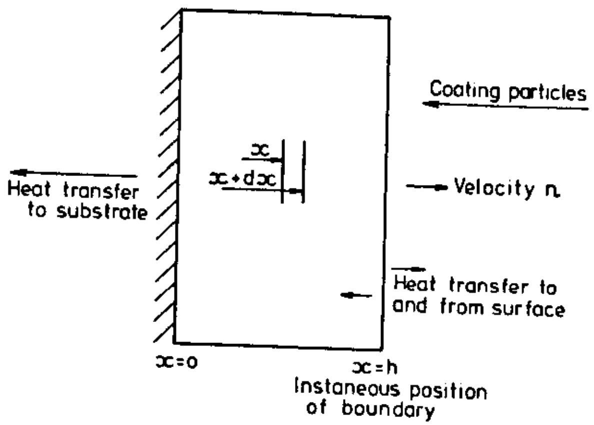

COATING UNDER DEPOSITION

Model Predictions

LECTURE 4 : SLIDE 9

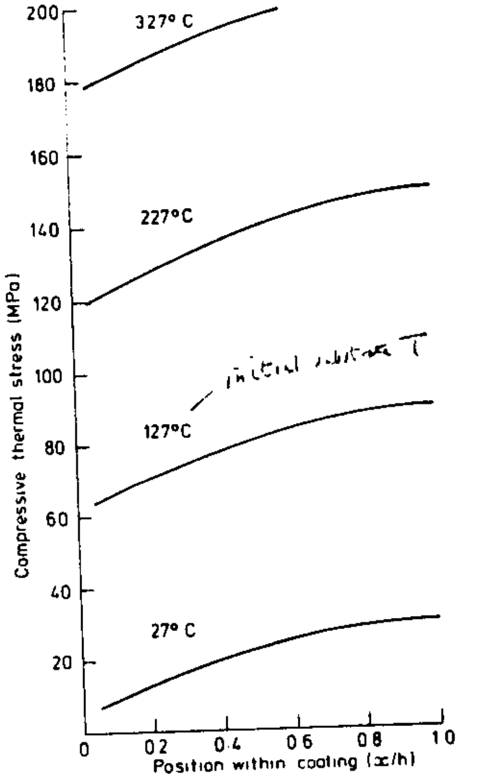

VARIATION OF INITIAL SUBSTRATE TEMPERATURE

All ZrO_2
Model prediction

Temp. of substrate dominates - influence coating stress through mismatch of expansion between coating and substrate

Very Sensitive to $T_{substrate}$

LECTURE 4 : SLIDE 10

Tension

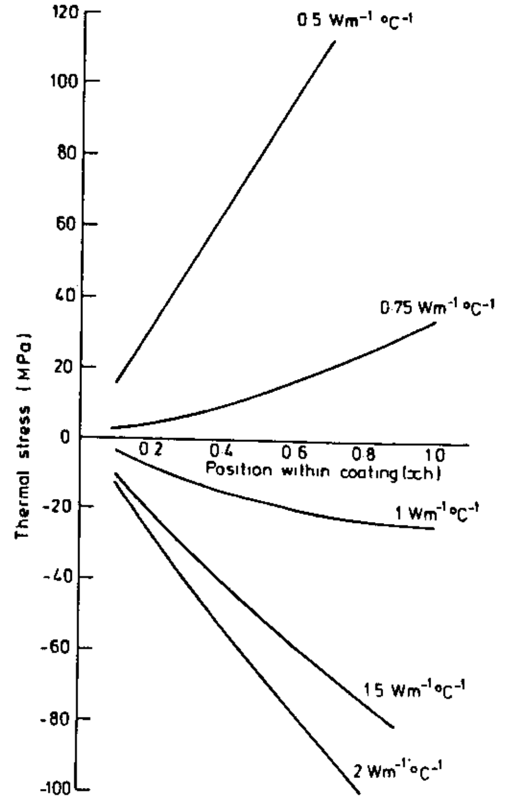

compression

VARIATION OF COATING THERMAL CONDUCTIVITY — 25% change can reverse sign of stress.

Rigid substrate: ideal ...

oxide particles in metal filter etc. could drastically affect this.

LECTURE 4 : SLIDE 11

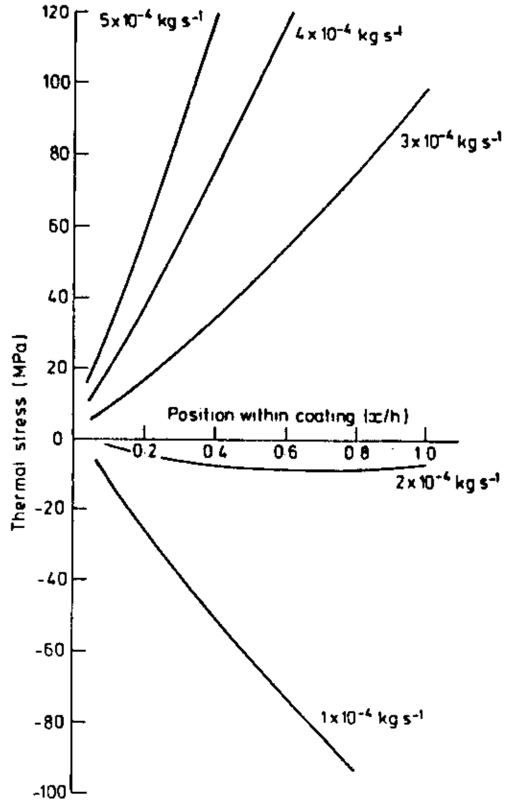

VARIATION OF DEPOSITION RATE

Again very sensitive

LECTURE 4 : SLIDE 12

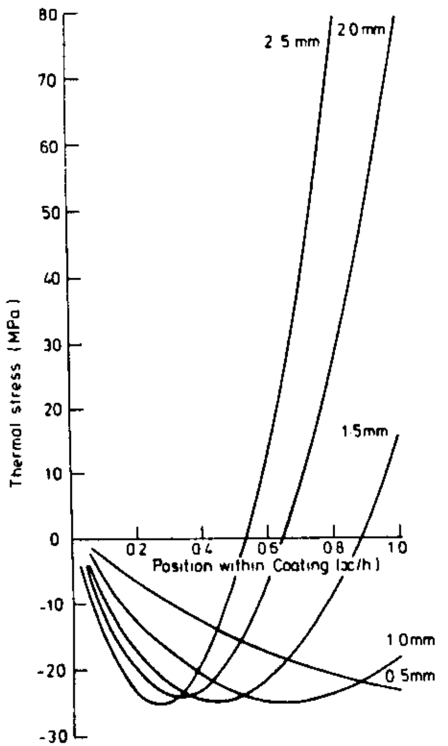

VARIATION OF COATING THICKNESS

Thick coatings can develope tensions

LECTURE 4 : SLIDE 13

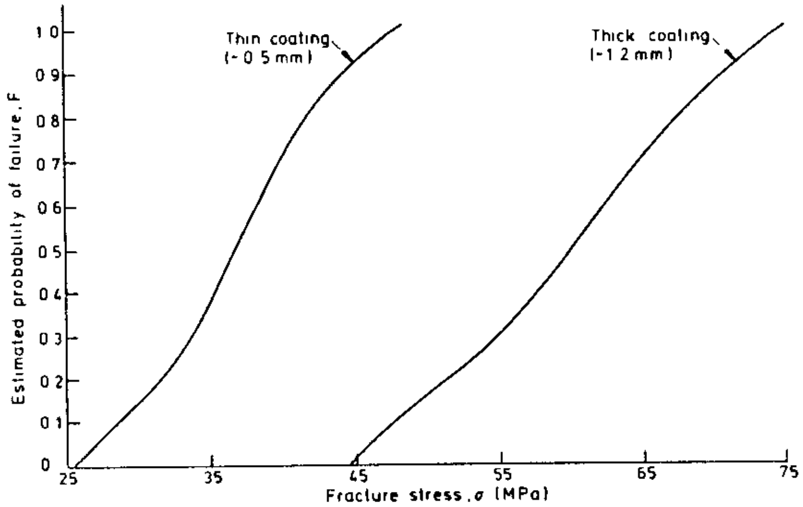

FRACTURE STRESS VERSUS ESTIMATED PROBABILITY OF FAILURE FOR TUNGSTEN COATINGS SPRAYED AT 76 g/min SHOWING THE EFFECT OF COATING THICKNESS

LECTURE 4 : SLIDE 14

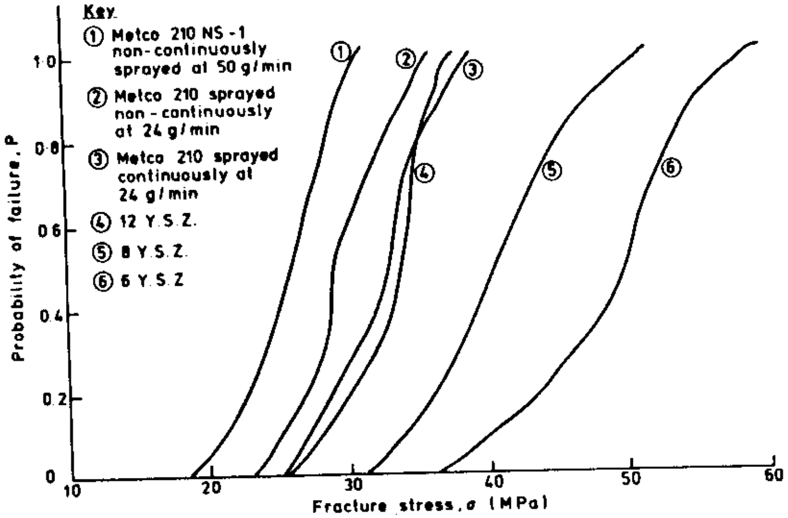

FRACTURE STRESS VERSUS ESTIMATED PROBABILITY OF FAILURE FOR VARIOUS PLASMA SPRAYED COATINGS

LECTURE 4 : SLIDE 15

PHYSICAL VAPOUR DEPOSITION: INTERFACES AND STRESSES

LECTURE 4 : SLIDE 16

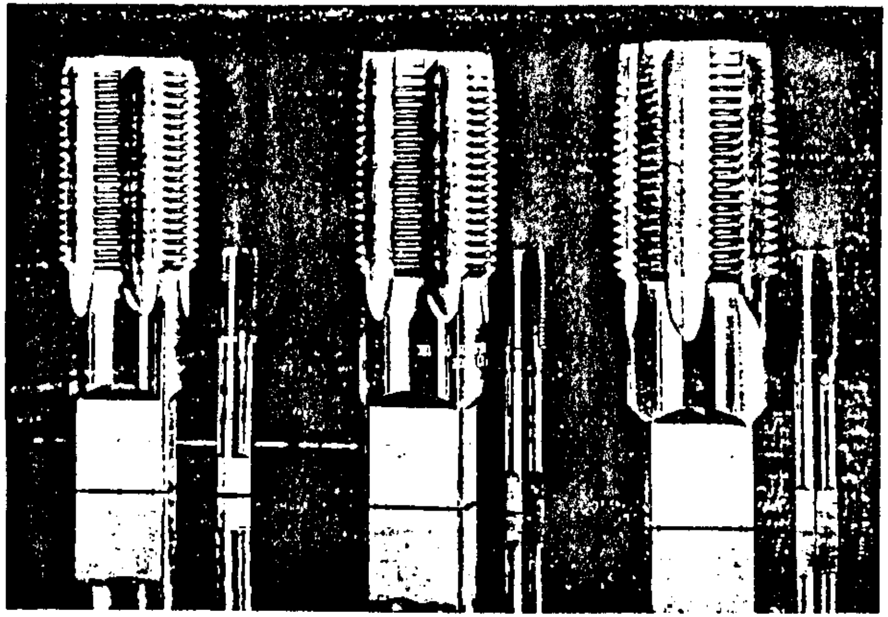

PVD TAPS for threading holes

LECTURE 4 : SLIDE 17

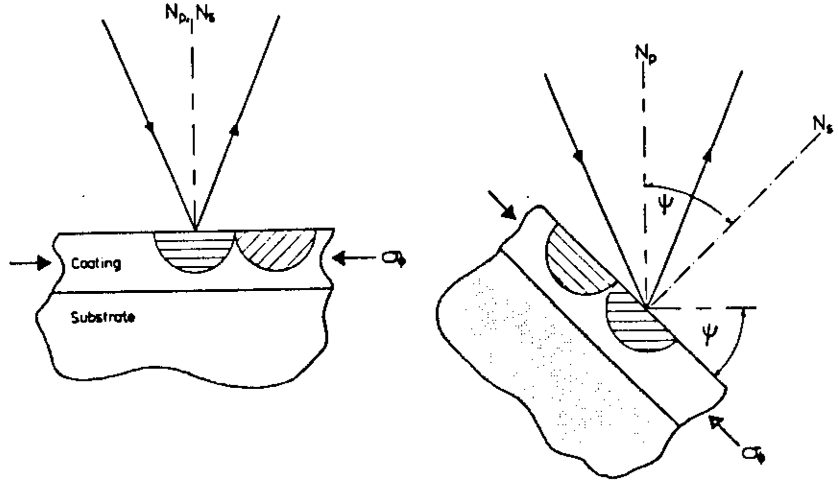

(a) Measurement of d_0 (b) Measurement of d_ψ

X-ray techniques for measuring stresses

LECTURE 4 : SLIDE 18

Xray

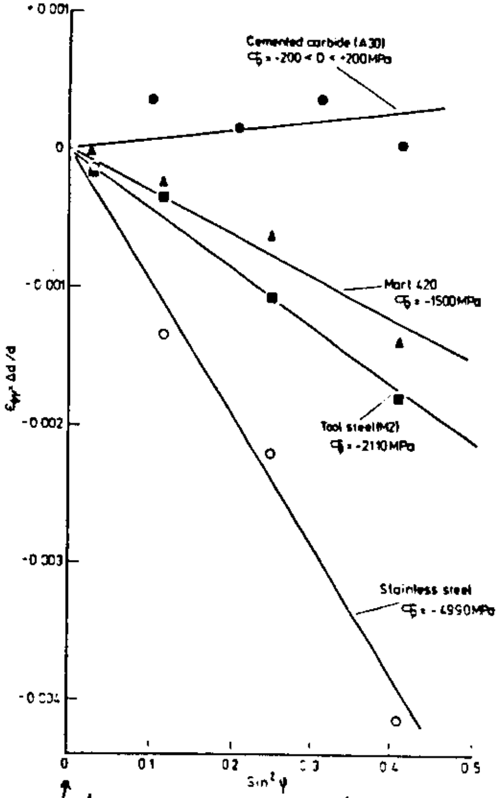

surface

Tilt angle (means of penetration)

TiN α = 9.3

SS α = 16

Tool Steel ~12

Martensite 420 ~12

Cemented Carbide ~4

Δα mismatch is crucial (explain)

Difference in expansion coeff. causes stresses in SIP (TiN)

LECTURE 4 : SLIDE 19

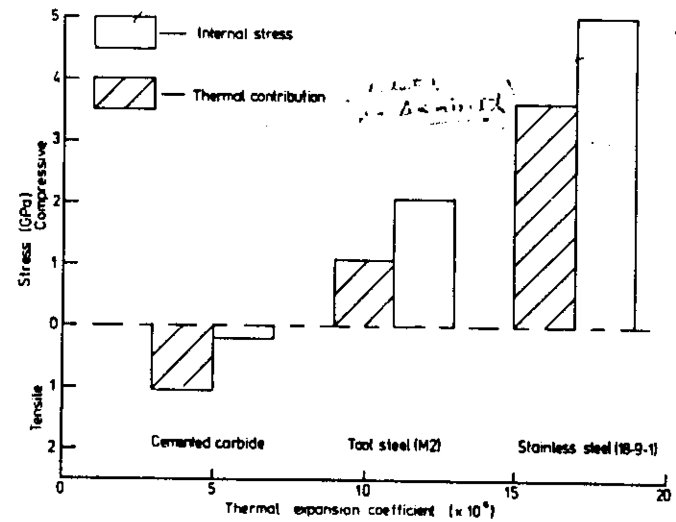

LECTURE 4 : SLIDE 20

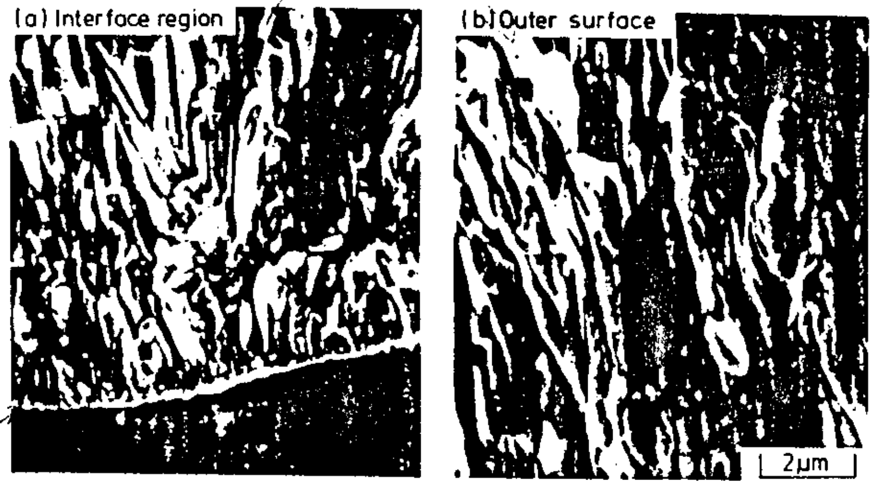

Variation of microstructure

— fine grained near interface → bigger towards free surface.

Columnar growth

This variation of microstructure is induced by variation of residual stress.

LECTURE 4 : SLIDE 21

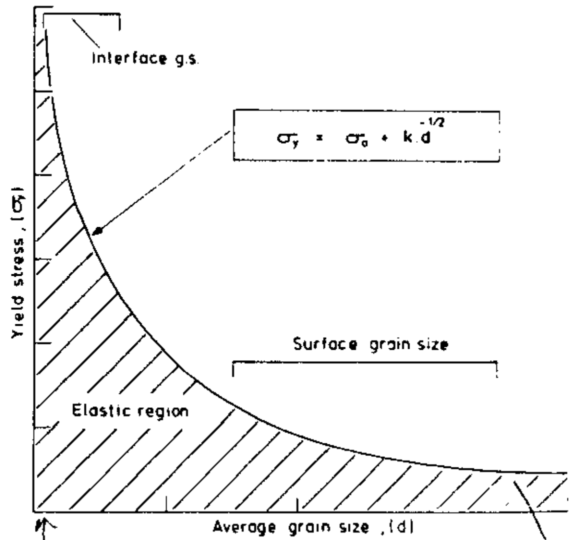

LECTURE 4 : SLIDE 22

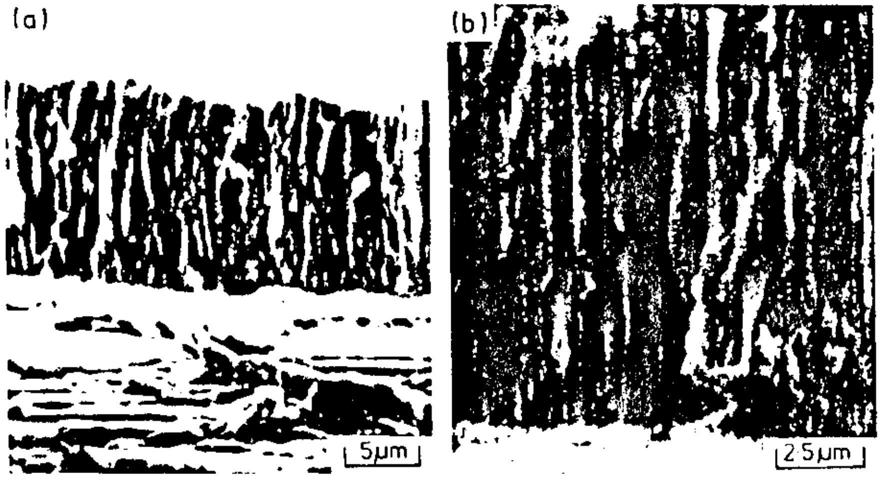

Mo on Mo.

[illegible]

X-ray [illegible] ~ 150 MPa

Huge mismatch [illegible] Mo on S.S.

LECTURE 4 : SLIDE 23

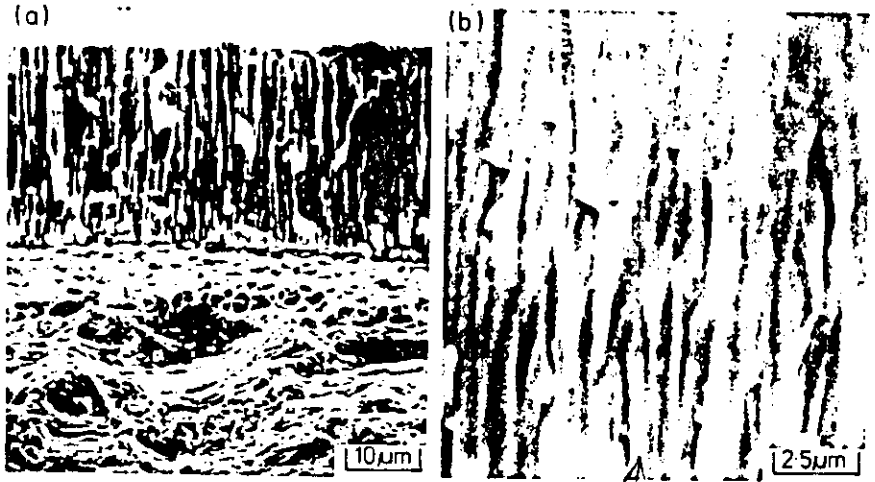

Pushed together

Very dense microstructure

Large mismatch

Mo on S.S.

Stress from X-rays ~ 1000 MPa

LECTURE 4 : SLIDE 24

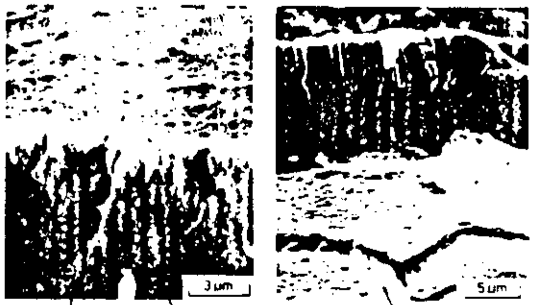

Carbide (W+Ti+C)

attacked substrate

NO BONDING IN THIS CASE

LECTURE 4 : SLIDE 25

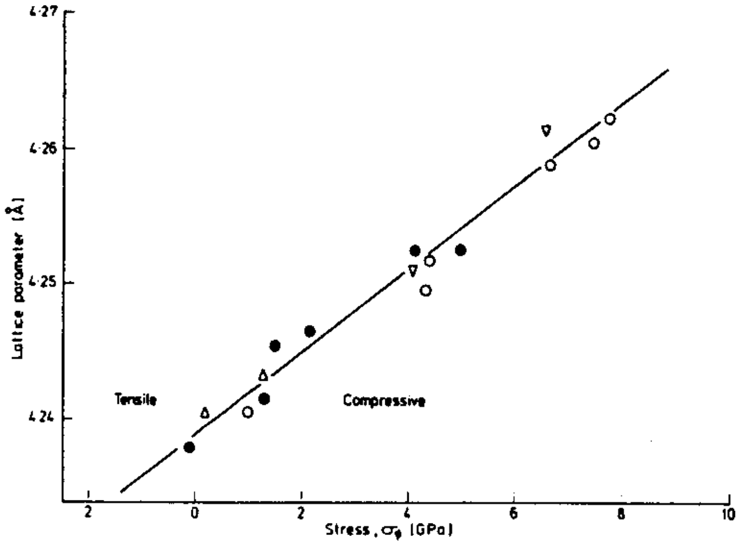

of TiN

(by X-ray)

compression

causes lattice parameter increase

Thought to be Argon

LECTURE 4 : SLIDE 26

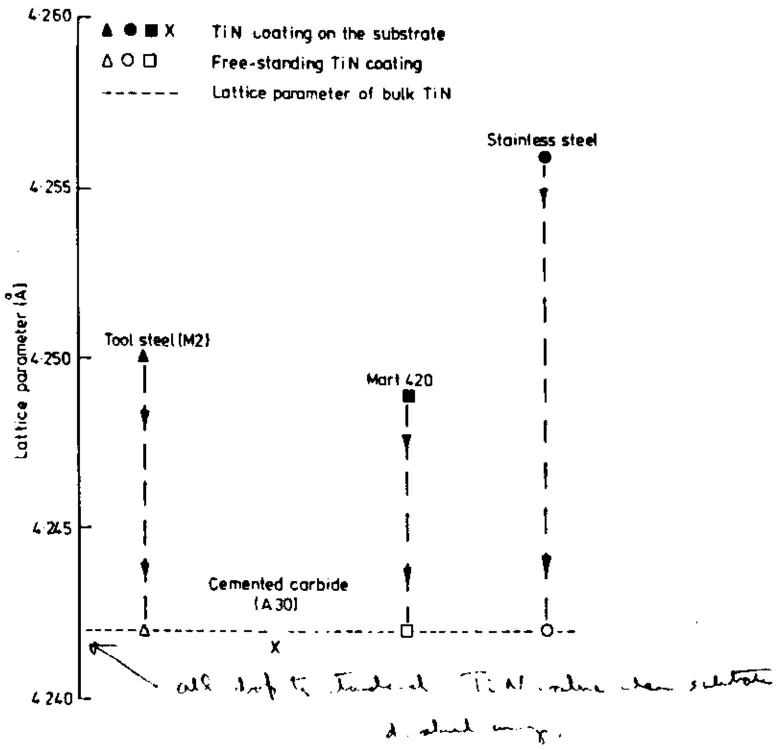

LECTURE 4 : SLIDE 27

FURTHER INTERFACE PHENOMENA

LECTURE 4 : SLIDE 28

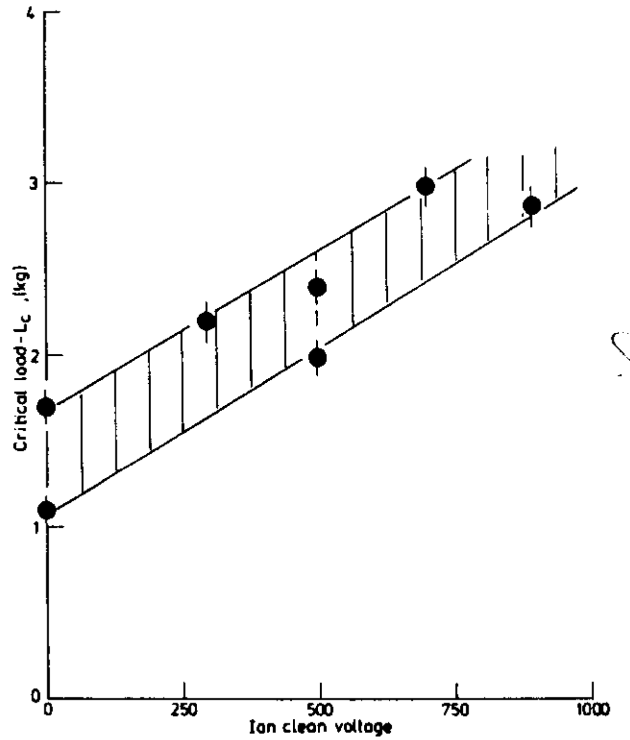

Scratch test

S/P

Pre cleaning of substrate surface is important

sputter [illegible] - instead of target

Adhesive bonding is [illegible] clean clean.

Scratch test

LECTURE 4 : SLIDE 29

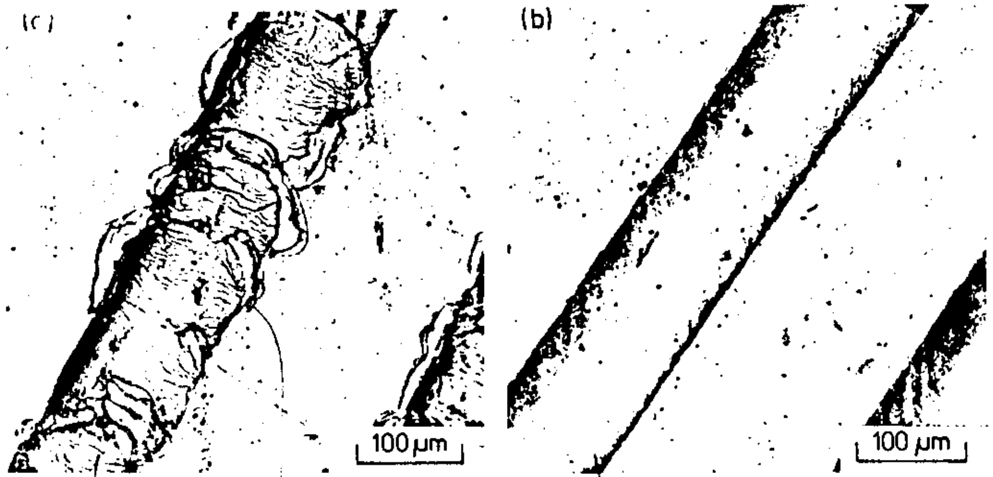

non ion cleaned substrate

chipping etc.

15 N load.

ion cleaned substrate

15 N load

ALSO

Ti interlayer effect

Then on to OVERHEADS

Stresses are important and can lead to failure

LECTURE 4 : SLIDE 30

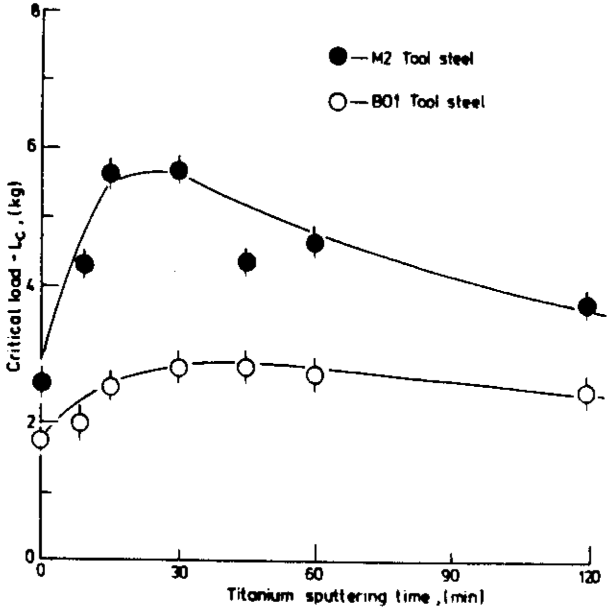

Glue effect of Ti — Max. Optimum glue thickness

Either getter or toughness effect

LECTURE 4 : SLIDE 31

Interfaces between coating & substrate

LECTURE 4 : SLIDE 32

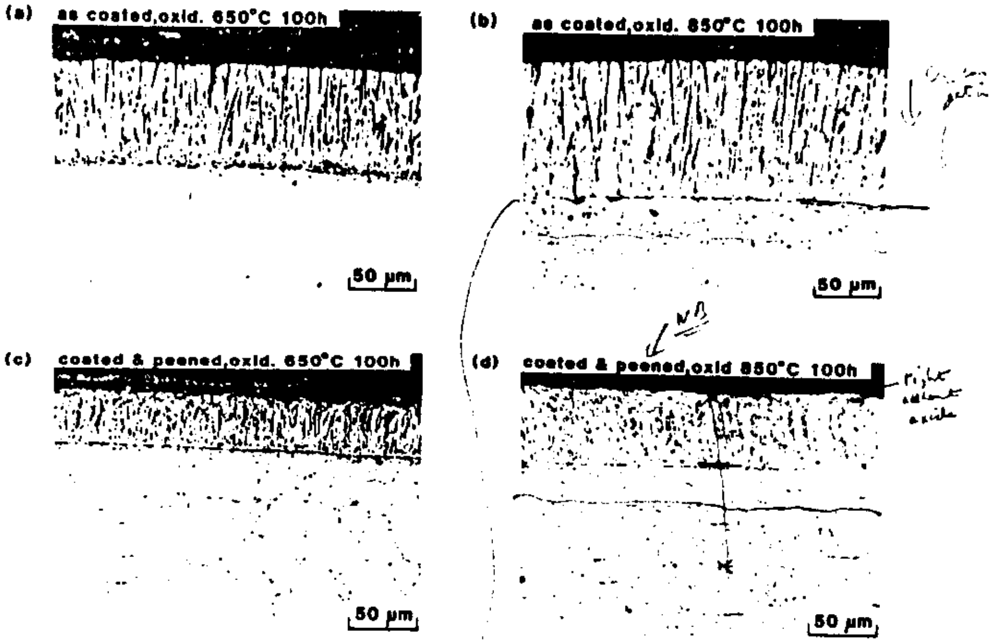

LECTURE 4 : SLIDE 33

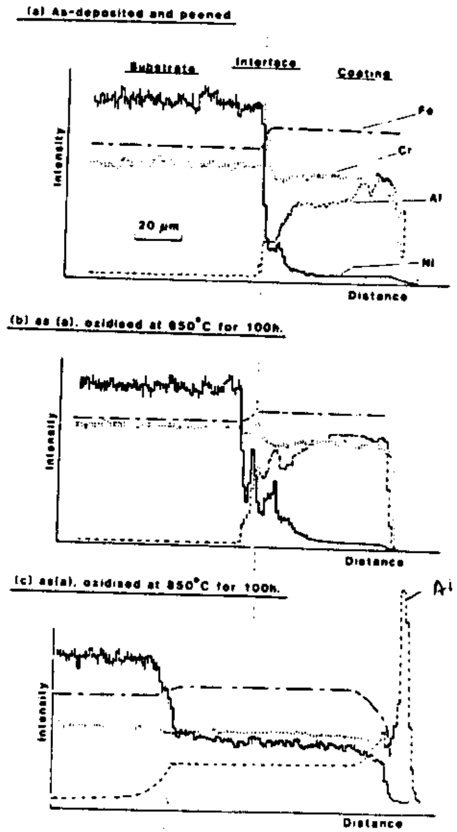

LECTURE 4 : SLIDE 34

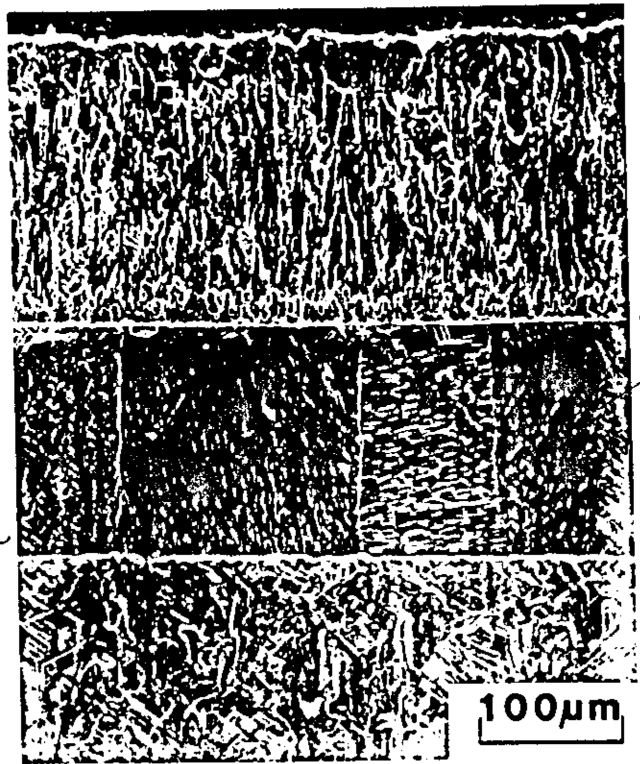

Deep etch micrograph

This banding observed to move down; then reverses as Al is depleted.

100 hrs at 1000°C

LECTURE 4 : SLIDE 35

passed

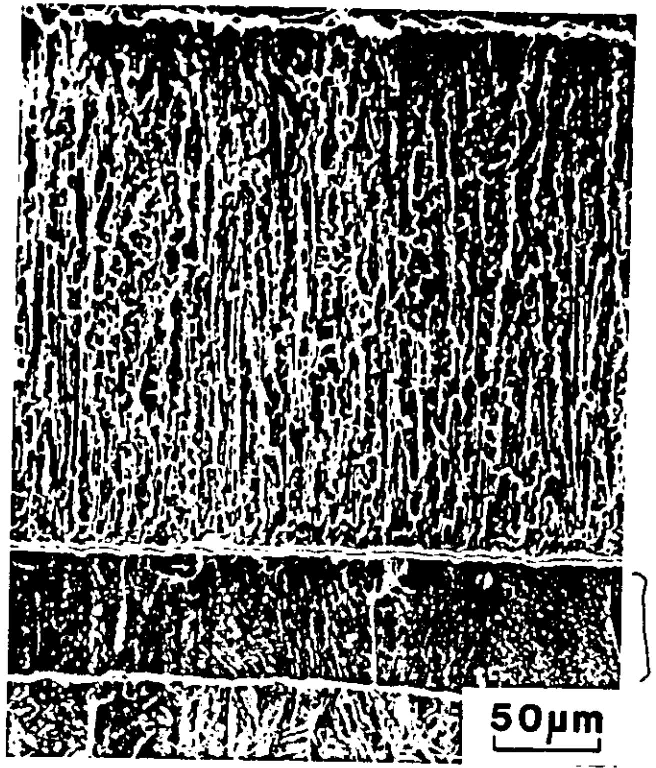

Al loss to substrate is bad thing ∴ it depletes

Al required to form Alumina at surface

Hence put in TiN as diffusion barrier

100 hrs at 1000°C

Reduced by 2½

LECTURE 4 : SLIDE 37

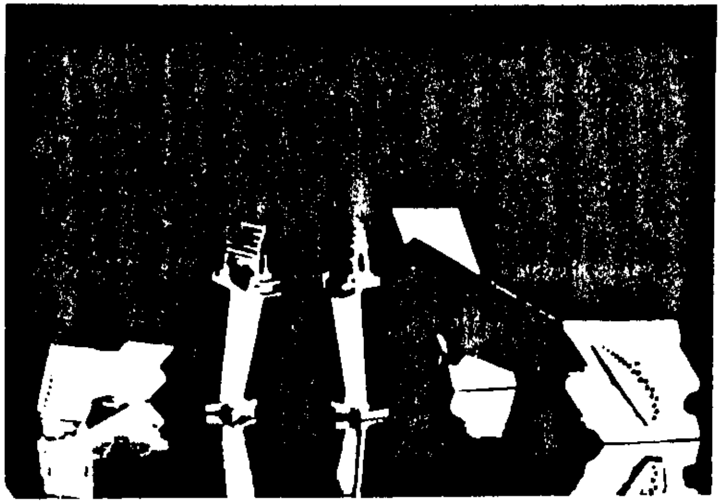

LECTURE 4 : SLIDE 38

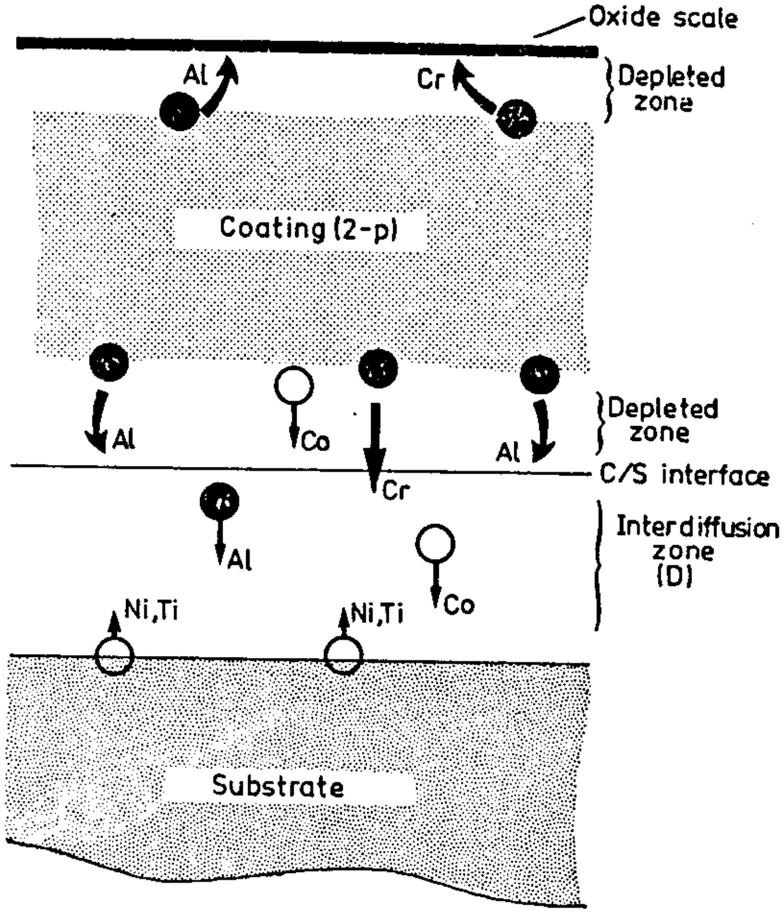

LECTURE 4 : SLIDE 39

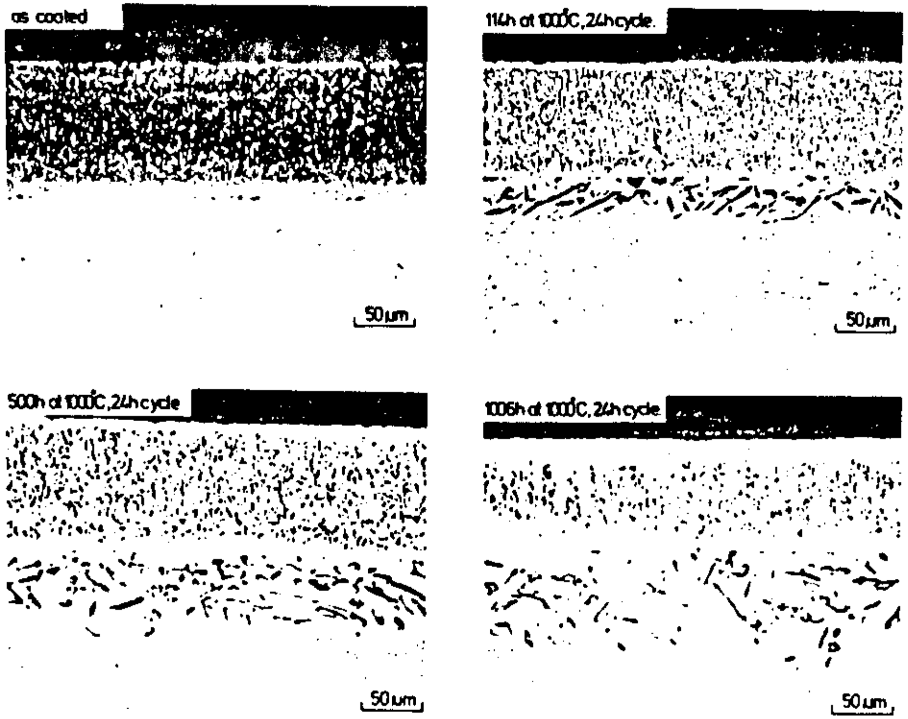

LECTURE 4 : SLIDE 40

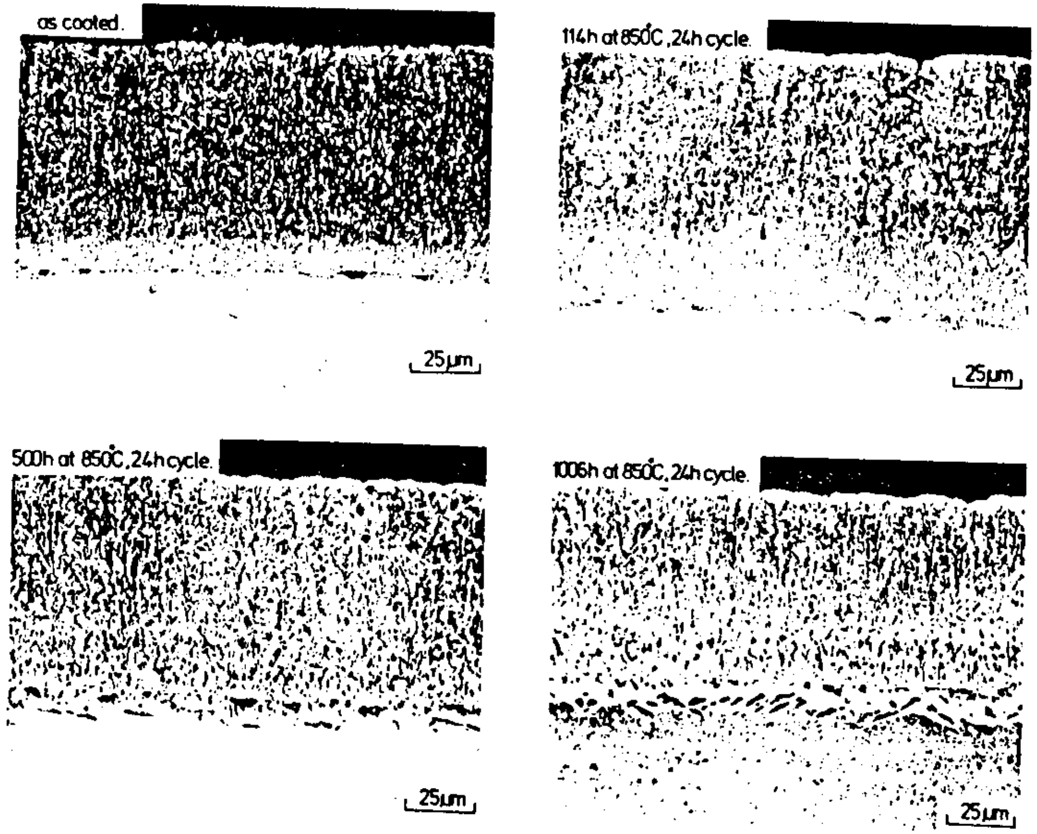

LECTURE 4 : SLIDE 41

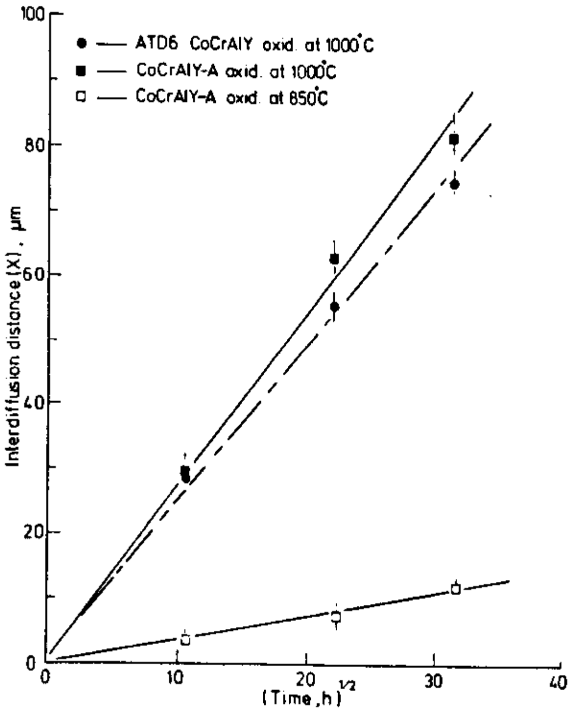

LECTURE 4 : SLIDE 42

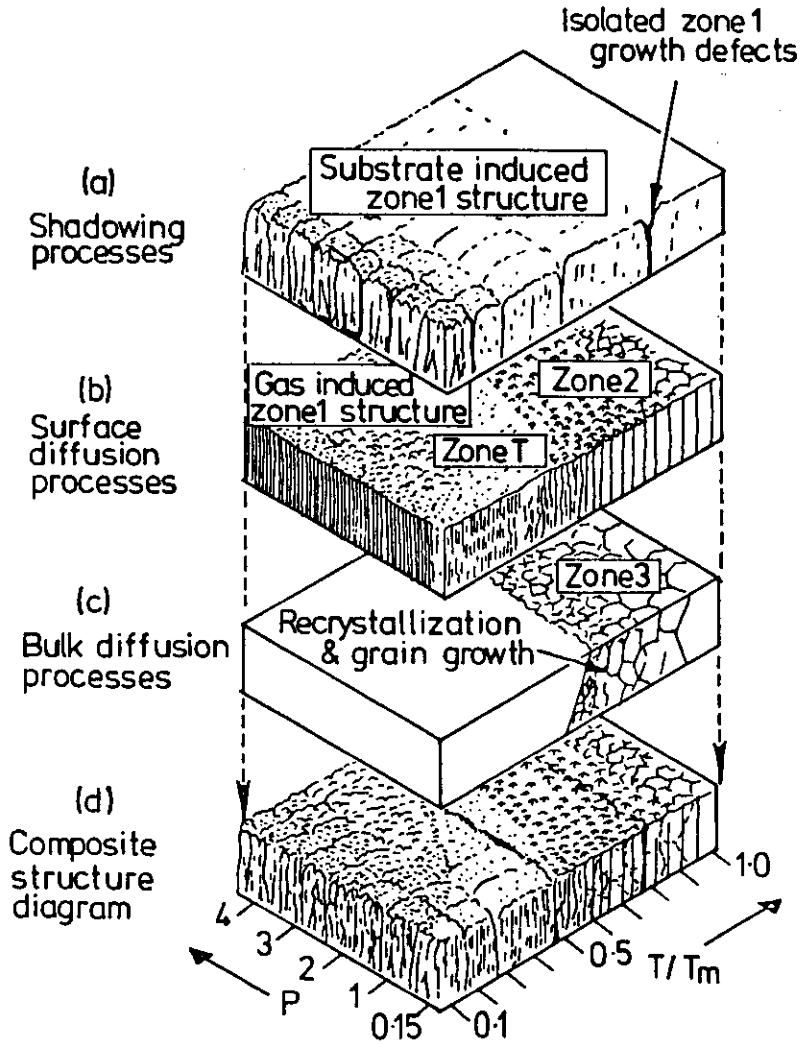

LECTURE 4 : SLIDE 43

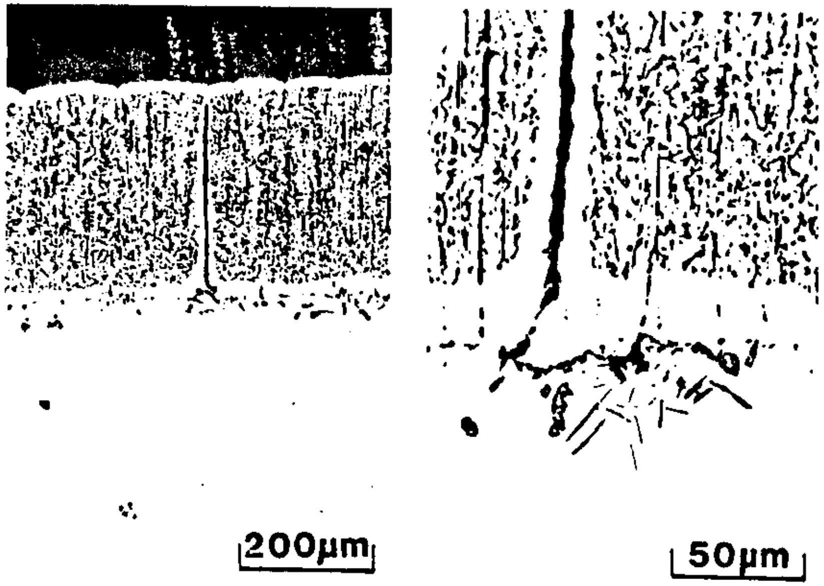

LECTURE 4 : SLIDE 44

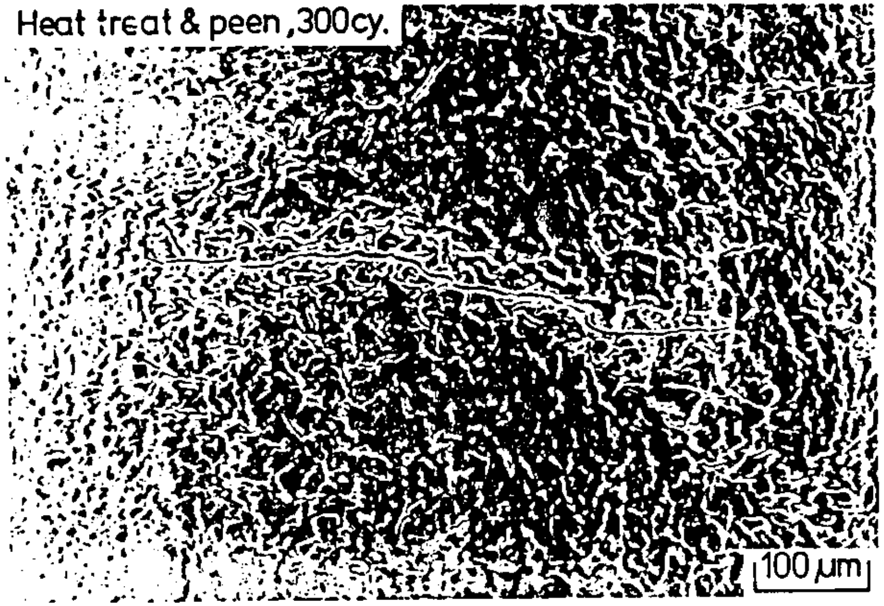

LECTURE 4 : SLIDE 45

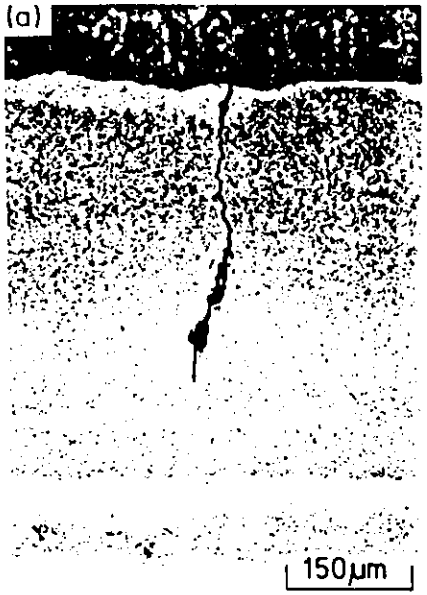

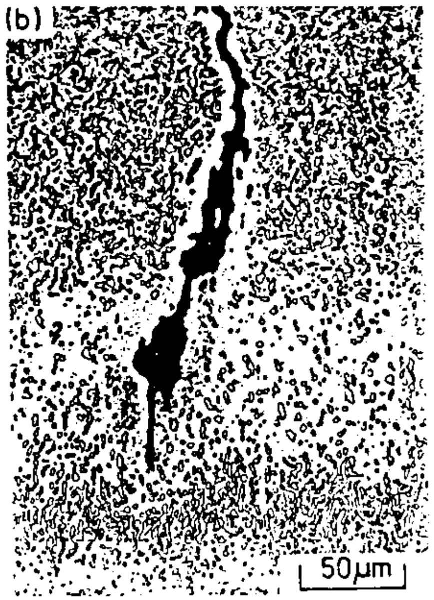

LECTURE 4 : SLIDE 46

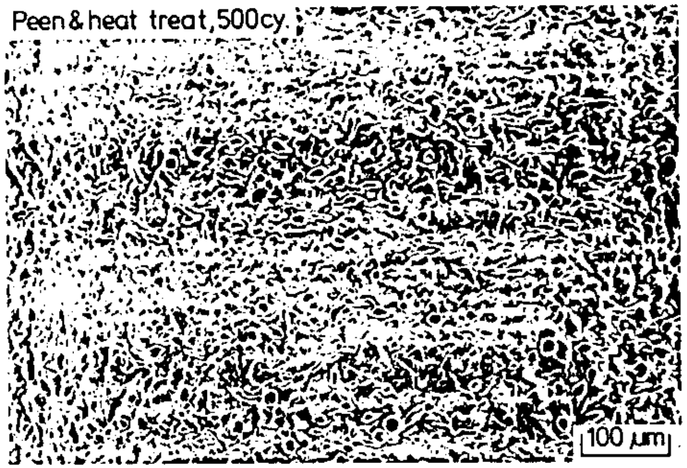

LECTURE 4 : SLIDE 47

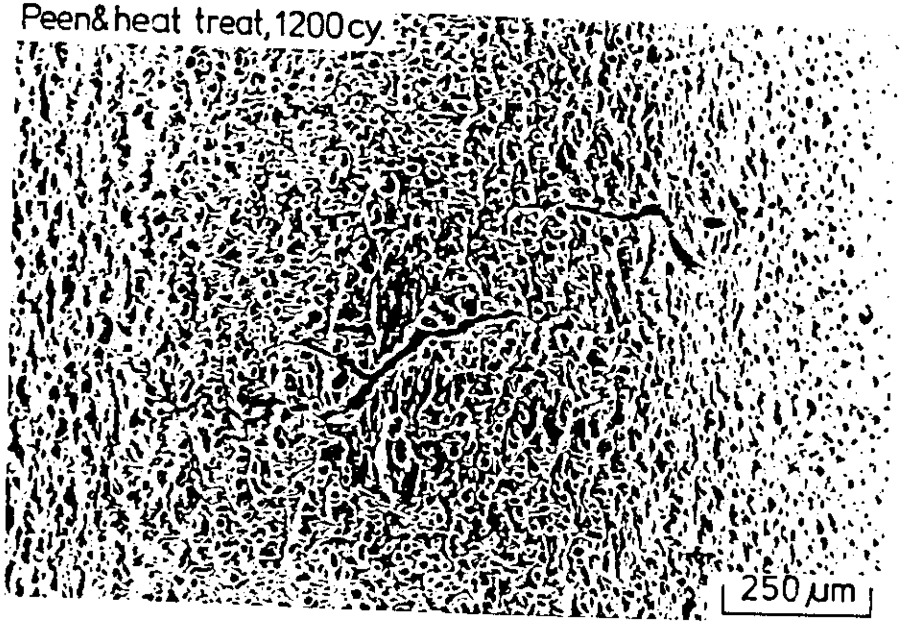

LECTURE 4 : SLIDE 48

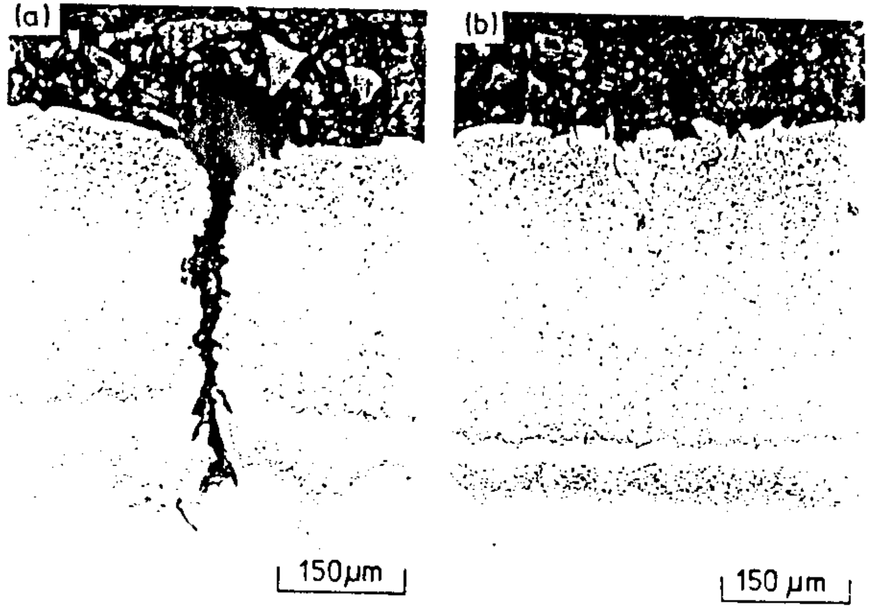

LECTURE 4 : SLIDE 49

SUMMARY

A. STRESSES IN COATINGS CAN BE SIGNIFICANT AND LEAD TO FAILURE

B. ADVANCED TECHNIQUES ARE REQUIRED TO MEASURE AND MODEL STRESSES

C. INTERFACES ARE VERY IMPORTANT

D. GROWTH DEFECTS ARE VERY IMPORTANT

Mechanism for the Spallation of Polycrystalline Coatings

R. Bullough, Harwell, U.K.

1. The Model

2. Analysis

3. Results

4. Conclusions and Required Development of the Model.

Model was originally developed for DIAMOND spallation - so for interest we give results for both DIAMOND and STAINLESS STEEL. Note however SIP DIAMOND COATINGS for 'HARD' device fabrication can now be made.

5 December 1986

MECHANISM FOR THE SPALLATION OF POLYCRYSTALLINE COATINGS

1. THE MODEL — (Previously developed with John Willis for diamond spallation)

2. ANALYSIS

3. RESULTS — (Computational help from Adrian Jones)

4. CONCLUSIONS AND REQUIRED DEVELOPMENT OF MODEL

MODEL

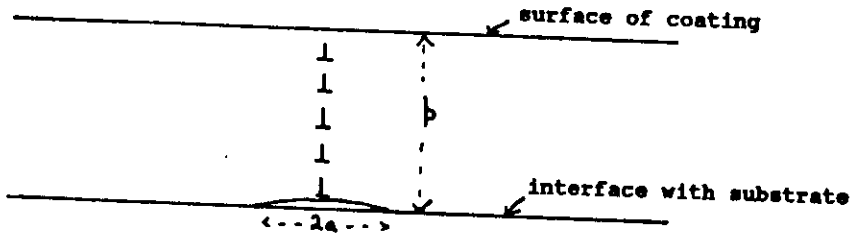

Terminating tilt boundary or wedge disclination extending to depth p below a free surface. At the moment we have no elastic or toughness distinction between coating and substrate.

Such a Tilt boundary

Localized representation of

A buckle in homogenously compressed coating

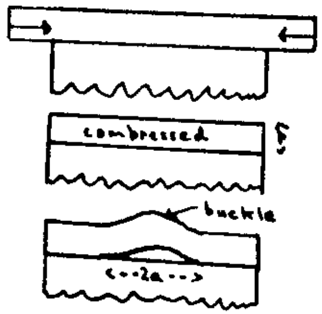

Q. How does crack size 'a' vary with p and buckle angle.

Representation of

A real terminating grain boundary (columnar grain)

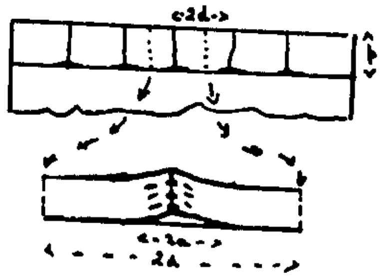

Q. How does crack size 'a' vary with p and tilt angle in comparison with grain size d. (High Bias).

Essential conjectures are that:

1. A critical microcrack size in the interface is needed for any cracking.

2. If $a > a_{min}$ the crack will open to stable size a_{max}.

3. As p increases the stresses in the interface at the core of the disclination will <u>increase</u>: a_{min} will decrease and a_{max} will increase.

<u>We wish to quantify above conjectures.</u>

<u>Spallation will occur if</u>

either

1. single interface crack reaches p in length.

or

2. Cracks join up from adjacent 'buckles' or from adjacent terminating grain boundaries (Latter case if $a_{max} = d$).

2. <u>Analysis</u>

<u>Step 1</u>

Stress field of single edge dislocation of strength b in a half space (x > 0).

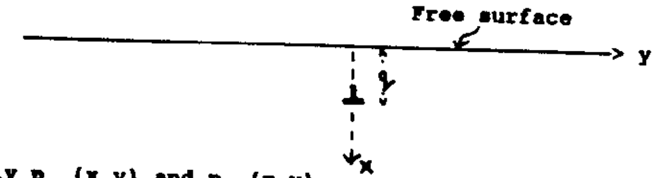

Need only $p_{xx}(x,y)$ and $p_{xy}(x,y)$.

$$p_{xx}^{(q)}(x,y) = A\left\{\frac{(x-q)[(x-q)^2-y^2]}{[(x-q)^2+y^2]^2} - \frac{(x+q)[(x+q)^2-y^2]}{[(x+q)^2+y^2]^2} + 2q\left[\frac{(3x+q)(x+q)^3-6x(x+q)y^2-y^4}{[(x+q)^2+y^2]^3}\right]\right\}$$

$$p_{xy}^{(q)}(x,y) = A\left\{\frac{y[(x-q)^2-y^2}{[(x-q)^2+y^2]} - \frac{y[(x+q)^2-y^2]}{[(x+q)^2+y^2]^2} + \frac{4qxy[3(x+q)^2-y^2]}{[(x+q)^2+y^2]^3}\right\}$$

where

$A = \mu b/2\pi(1-\nu)$; μ = shear modulus, ν = Poisson's Ratio.

Note these stresses (tractions) vanish on $x = 0 \rightarrow$ Free Surface.

Step 2

Linear superposition of N such dislocation stresses yield stresses associated with terminating tilt boundary:

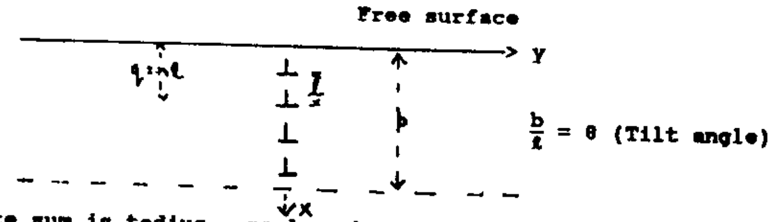

Finite sum is tedius - replace by continuous distribution:

$$p^T_{xx}(x,y) = \sum_{n=1}^{N} p^{(n\ell)}_{xx}(x,y)$$

$$= \frac{1}{\ell}\int_0^p p^{(q)}_{xx}dq = \frac{A\theta}{b}\left\{ \frac{1}{2}\ln\left[\frac{(x+p)^2+y^2}{(x-p)^2+y^2}\right] - \frac{y^2}{[(x-p)^2+y^2]} + \frac{2x^2-2x(x+p)+y^2}{[(x+p)^2+y^2]} + \frac{4xy^2p}{[(x+p)^2+y^2]^2}\right\}$$

$$p^T_{xy}(x,y) = \sum_{n=1}^{N} p^{(n\ell)}_{xy}(x,y)$$

$$= \frac{1}{\ell}\int_0^p p^{(q)}_{xy}dq = \frac{A\theta}{b}\left\{ \frac{(x-p)y}{[(x-p)^2+y^2]} + \frac{(x+p)y}{[(x+p)^2+y^2]} - \frac{6xy}{[(x+p)^2+y^2]} + \frac{4xy[x(x+p)+y^2]}{[(x+p)^2+y^2]^2}\right\}$$

Note stresses again vanish on free surface $x = 0$.

Step 3

Imagine slit crack immediately below tilt boundary in $x = p$ plane parallel to z-axis of length 2a

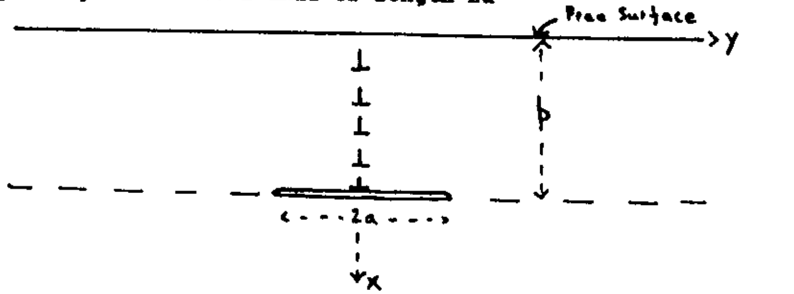

Stress intensity factors K_I and K_{II} at tip of such a crack:

$$K_I = 2\left[\frac{a}{\pi}\right]^{1/2}\int_0^a \frac{p^T_{xx}(p,y)dy}{[a^2-y^2]^{1/2}} \qquad \text{Mode I}$$

$$K_{II} = \frac{2}{[\pi a]^{1/2}}\int_0^a \frac{y\,p^T_{xy}(p,y)dy}{[a^2-y^2]^{1/2}} \qquad \text{Mode II}$$

Crack extension force

$$G(a) = \frac{1-\nu}{2\mu}\left[K_I^2+K_{II}^2\right]$$

Integrals are analytic:

We find

$$G(a) = \frac{\mu\theta^2 p}{8\pi(1-\nu)} f(r)$$

$$f(r) = r\left\{\left[\ln\left(\frac{2+(4+r^2)^{1/2}}{r}\right) - \frac{2(6+r^2)}{(4+r^2)^{3/2}}\right]^2 + \frac{4r^3}{(4+r^2)^3}\right\}$$

where $r = a/p$.

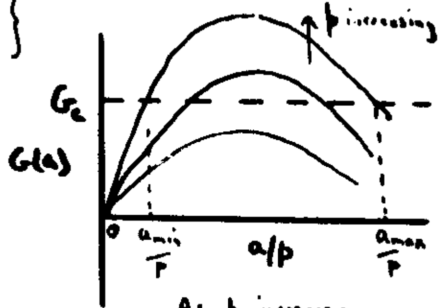

As p increases
a_{min} decreases
a_{max} increases
G(a) will eventually reach G_c!

Propagation will occur if

$$G(a) \geq G_c$$

For brittle material (Diamond) $G_c = 2\gamma \sim \frac{\mu b}{10}$.

Finally:

$$\frac{G(a)}{G_c} = 0.6\left[\frac{\mu b}{10G_c}\right]\frac{p}{b}\theta^2 f(r) \qquad (\nu = 1/3)$$

$$G_c = \frac{2}{3\mu}K_c^2$$

Thus in terms of toughness K_c:

$$\frac{G(a)}{G_c} = 0.6\left[\frac{3\mu^2 b}{20K_c^2}\right]\frac{p}{b}\theta^2 f(r) \xrightarrow{\text{Extreme brittle}} 0.6\,\frac{p}{b}\theta^2 f(r).$$

3. **Results**

1. **Extreme brittle material (Diamond)**

$$\mu = 550\ \text{GPa},\ K_c = 4.3\ \text{MPa}\sqrt{m}$$

2. **Low alloy steel (2¼Cr 1Mo)**

$$\mu = 83\ \text{GPa},\ K_c = 23\ \text{MPa}\sqrt{m}$$

NEXT 4 TRANS: $\frac{G(a)}{G_c}$ versus $\frac{a}{p}$ for range of p, θ^2

a_{min} and a_{max} obtained.

$\mu = 550$ GPa
$K_c = 4 \cdot 3$ MPa$\sqrt{m}$

$\theta = 1°$

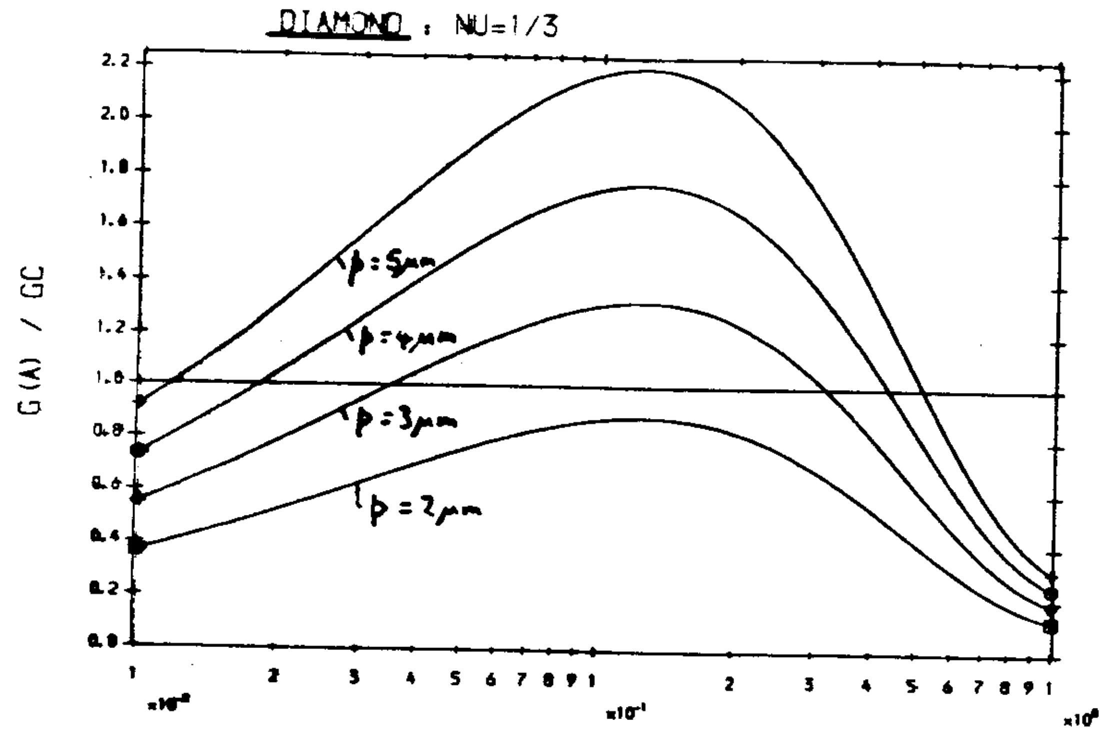

	P (MIC.)	TH (DEG.)	AMIN (MIC.)	AMAX (MIC.)
■	2.000	1.000	0.000	0.000
●	3.000	1.000	0.105	0.949
●	4.000	1.000	0.072	1.733
+	5.000	1.000	0.059	2.578

← 590 Å

$p = 15\mu m$, $a_{min} \sim 5$Å!, $a_{max} \simeq 15\mu m$.

-67-

$\mu = 550$ GPa
$K_c = 4 \cdot 3$ MPa$\sqrt{m}$

$p = 5\mu m$
$1 \cdot 2° \geq \theta \geq 0 \cdot 8°$

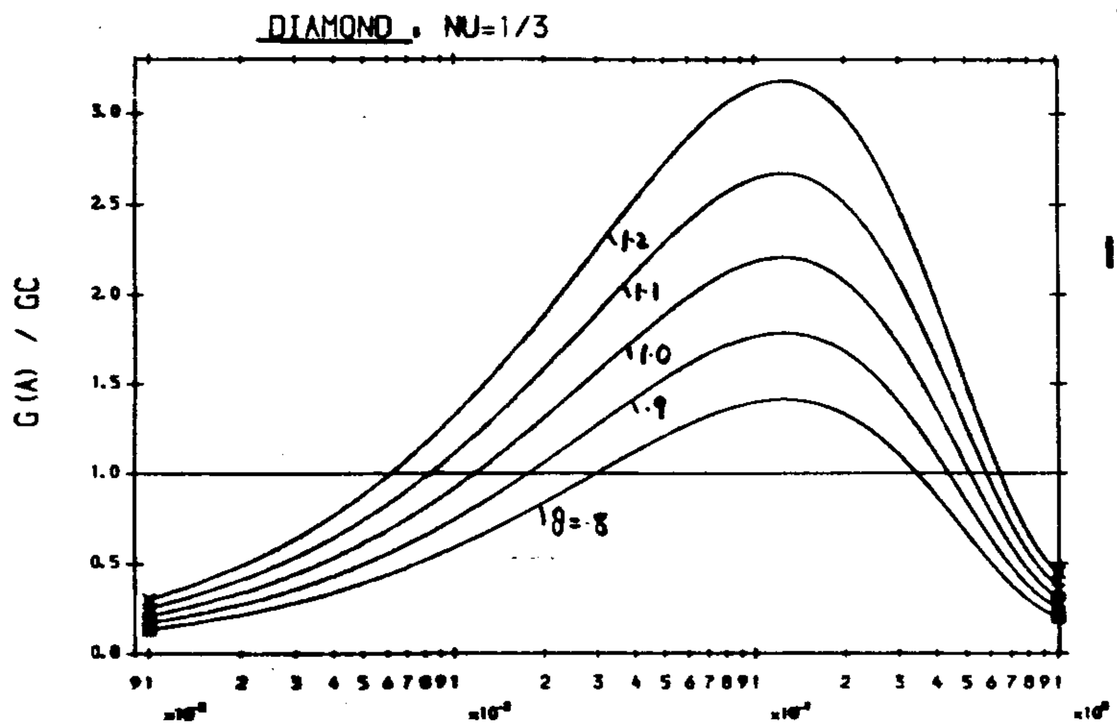

	P (MIC.)	TH (DEG.)	AMIN (MIC.)	AMAX (MIC.)
■	5.000	0.800	0.140	1.721
●	5.000	0.900	[illegible]	2.190
●	5.000	1.000	[illegible]	2.578
+	5.000	1.100	[illegible]	2.919
x	5.000	1.200	[illegible]	3.230

~ 3μÅ

-68-

$\mu = 83 GPa$
$K_c = 23 MPa\sqrt{m}$

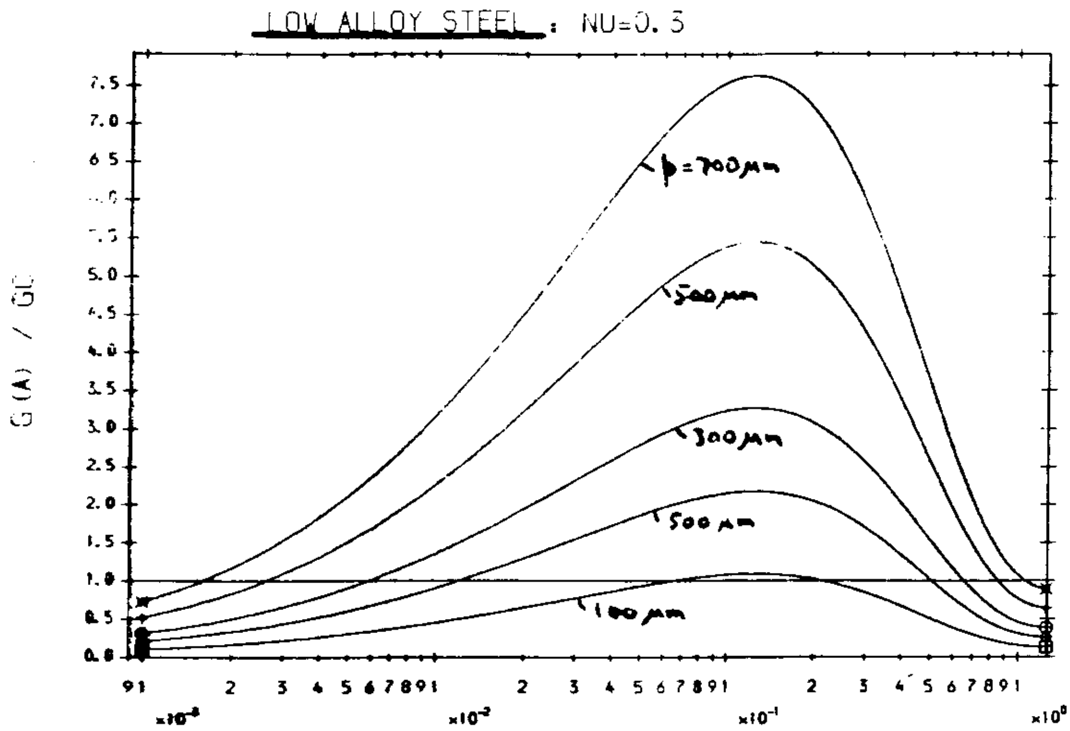

	P (MIC.)	TM (DEG.)	AMIN (MIC.)	AMAX (MIC.)
⊞	100.000	0.000	6.470	21.613
◆	200.000	0.000	2.420	102.141
●	300.000	0.000	1.800	196.723
+	500.000	0.000	1.350	428.229
x	700.000	0.000	1.120	741.862

$\mu = 83 GPa$
$K_c = 23 MPa\sqrt{m}$

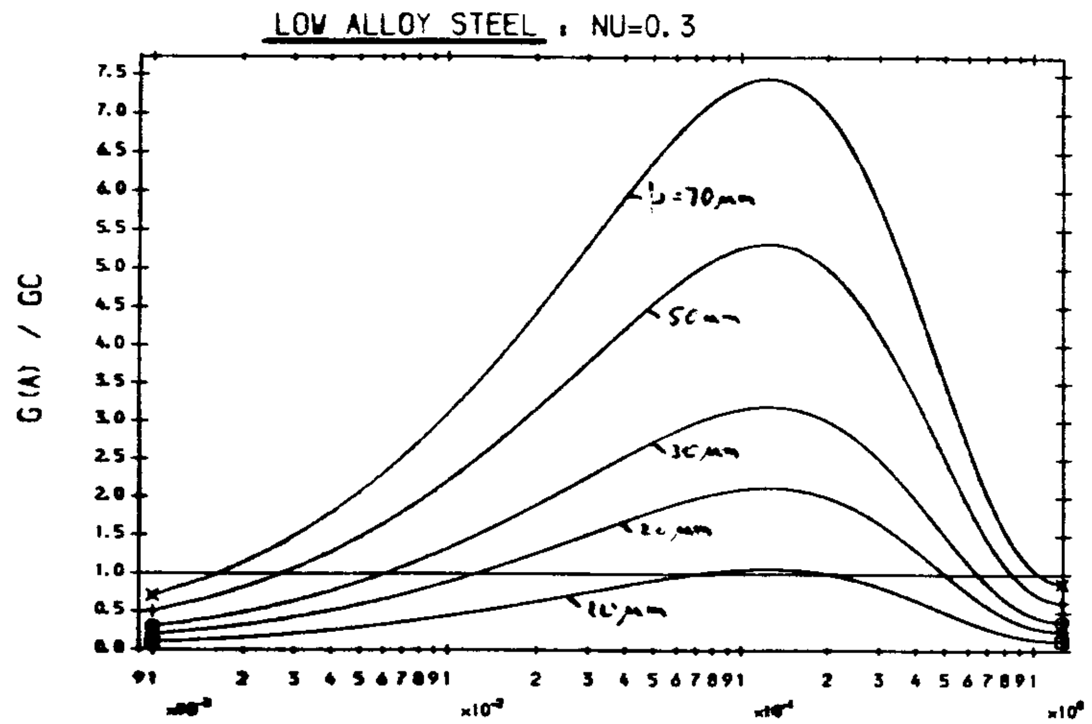

	P (MIC.)	TM (DEG.)	AMIN (MIC.)	AMAX (MIC.)
⊞	[illegible]	25.000	[illegible]	2.[illegible]
◆	[illegible]	[illegible]	[illegible]	[illegible]
●	[illegible]	[illegible]	[illegible]	[illegible]
+	[illegible]	[illegible]	[illegible]	[illegible]
x	70.000	[illegible]	[illegible]	72.[illegible]

4. Conclusions and Required Developments of Model

$$\frac{G(a)}{G_c} = 0.6 \left[\frac{3\mu^2 b}{20K_c^2}\right] \frac{p}{b}\, \theta^2\, f(r)$$

(a) Diamond has high μ, low $K_c \rightarrow \frac{G(a)}{G_c}$ easily reaches unity.

(b) Steel has both lower μ and higher K_c.

(c) $\frac{G(a)}{G_c} = p$.
a_{min} drops and a_{max} rises as p increases.

(d) Usually $\mu_{coating} >> \mu_{substrate}$
$K_{c(coating)} << K_{c(substrate)}$ Helps to enhance spallation

Composite problem needs solving but surely somewhere between homogeneous DIAMOND and homogeneous STEEL.

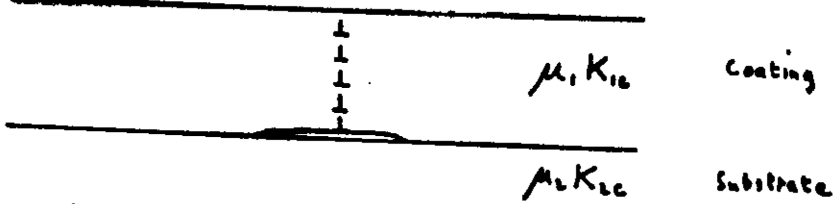

(e) Can see importance of intermediate high toughness layer.

(e) Ideal problem to solve: